An Extended Kalman-Bucy Filter for Atmospheric Temperature Profile Retrieval with a Passive Microwave Sounder

W. H. LEDSHAM AND D. H. STAELIN

Department of Electrical Engineering and Computer Science, and Research Laboratory of Electronics, Massachusetts Institute of Technology, Cambridge 02139

(Manuscript received 28 December 1978)

ABSTRACT

An extended Kalman-Bucy filter has been implemented for atmospheric temperature profile retrievals from observations made using the Scanned Microwave Spectrometer (SCAMS) instrument carried on the Nimbus 6 satellite. This filter has the advantage that it requires neither stationary statistics in the underlying processes nor linear production of the observed variables from the variables to be estimated. This extended Kalman-Bucy filter has yielded significant performance improvement relative to multiple regression retrieval methods.

A multi-spot extended Kalman-Bucy filter has also been developed in which the temperature profiles at a number of scan angles in a scanning instrument are retrieved simultaneously. These multi-spot retrievals are shown to outperform the single-spot Kalman retrievals.

1. Introduction

Atmospheric temperature profiles are presently being sensed from satelliteborne spectrometers observing the earth's atmosphere. These instruments view the earth's atmosphere in various molecular absorption bands, most notably those of the uniformly mixed gases carbon dioxide and oxygen. By varying the wavelength at which the observations are made, the pressure level where the thermal radiation primarily originates may be selected.

The area of atmospheric profile retrieval is sometimes segmented into two problems: the forward problem and the inverse problem. The forward problem is the process of determining the radiance set that would be observed by a sensor given a perfect knowledge of the state of the atmosphere. The inverse problem is concerned with the determination of the state of the atmosphere given a noisy radiance set observed with a sensor. A number of statistical and non-statistical methods have been advanced for the inversion of radiance sets. These methods have included multiple regression methods such as the statistical D method (Rosenkranz *et al.*, 1972; Waters *et al.*, 1975), the minimum information technique (Fleming and Smith, 1972) and various relaxation techniques.

The purpose of this paper is to introduce a powerful technique to the problem of temperature profile inversion: the extended Kalman-Bucy filter. The extended Kalman-Bucy filter is a statistical estimation technique that requires neither stationary statistics nor linear production of the observed variables from the variables to be estimated. The filter enhances performance by using the entire observation history in its inversion process. In a scanning instrument, the temperature profiles at a number of look angles may be inverted simultaneously. This simultaneous or bulk inversion ability is unique among presently used inversion schemes in that the inversion at a single look angle is affected by both previous and adjacent data cells. The bulk inverter makes optimum use of the differences in weighting functions with scan angle and any *a priori* knowledge of the statistical variation of the earth's atmosphere from point to point.

In order to explore these advantages of the extended Kalman-Bucy filter, it has been implemented as a temperature inverter for the SCAMS instrument carried on the Nimbus 6 satellite. The SCAMS instrument is a scanning microwave spectrometer that observes the upwelling radiation from the earth at five frequencies (Staelin *et al.*, 1975, 1977). Three of these frequencies (52.85, 53.85 and 55.45 GHz) are in an oxygen absorption complex and are primarily useful for temperature profiling. The remaining two (22.235 and 31.65 GHz) are used primarily to produce estimates of liquid water and water vapor columns over ocean and surface characteristics over ice pack or land (Grody *et al.*, 1977, Staelin *et al.*, 1977).

2. Radiative transfer basis of passive remote sensing

The basis of the ability to perform passive remote temperature profile sensing derives from the fact that

0021-8952/78/1023-1033$05.50

by careful selection of observation frequencies, thermal radiation originating from different levels in the atmosphere may be measured. In order to define a temperature-profile-inverting Kalman-Bucy filter, it is necessary to quantify the manner in which the measurement is produced. This quantification is often termed the observation or modulation matrix in the literature of Kalman-Bucy filtering and will be shown to correspond to the discrete weighting function of the remote sensing literature.

The received flux seen by a downward-looking observer through a non-scattering medium is approximately given by

$$I(\nu)=\int_0^H B[\nu,T(h)]K(\nu,h)\times\{\tau(h,H)+R(\nu,T_{\text{surf}})\tau(0,h)\tau(0,H)\}dh+\{1-R(\nu,T_{\text{surf}})\}\tau(0,H)B(\nu,T_{\text{surf}})+R(\nu,T_{\text{surf}})\tau(0,\infty)\tau(0,H)I_{\text{sky}}(\nu), \quad (1)$$

where $B(\nu,T)$ is the Planck function at frequency ν and temperature T, H is the height of the observer above the surface, h and h' trace a ray along the viewing angle, $I(\nu)$ is the received flux at frequency ν, $I_{\text{sky}}(\nu)$ the flux from cold space at frequency ν, $K(h,\nu)$ the absorption due to all species at height h and frequency ν, $R(\nu,T_{\text{surf}})$ the reflectivity of the surface boundary at frequency ν and temperature T_{surf}, $T(h)$ the temperature at height h, T_{surf} the temperature of the surface boundary and $\tau(h_1,h_2)$ the extinction of the atmosphere along the viewing angle equal to

$$\tau(h_1,h_2)=\exp\left[-\int_{h_1}^{h_2}K(\nu,h')dh'\right]. \quad (2)$$

For microwave frequencies, it is permissible to invoke the Raleigh-Jeans approximation to simplify (1) (e.g., Staelin, 1969). It then becomes

$$T_B(\nu)=\int_0^H T(h)K(\nu,h)\times\{\tau(h,H)+R(\nu,T_{\text{surf}})\tau(0,h)\tau(0,H)\}dh+\{1-R(\nu,T_{\text{surf}})\}\tau(0,H)T_{\text{surf}}+R(\nu,T_{\text{surf}})\tau(0,H)\tau(0,\infty)T_{\text{sky}}, \quad (3)$$

where $T_B(\nu)$ is the received brightness temperature and T_{sky} the brightness temperature of cold space. It is often convenient to combine a number of the terms in (3) to yield an equation of the form

$$T_B(\nu)=\int_0^H T(h)W[h,\nu,R(\nu,T_{\text{surf}})]dh+T_{\text{surf}}W_{\text{surf}}[\nu,R(\nu,T_{\text{surf}})]+T_{\text{sky}}W_{\text{sky}}[\nu,R(\nu,T_{\text{surf}})], \quad (4)$$

where $W(h,\nu,R)$ is often called the continuous temperature weighting function and is equal to

$$W(h,\nu,R(\nu,T_{\text{surf}}))=K(\nu,h)[\tau(h,H)+R(\nu,T_{\text{surf}})\tau(0,h)\tau(0,H)]. \quad (5)$$

In a similar manner, $W_{\text{surf}}(\nu,R)$ and $W_{\text{sky}}(\nu,R)$ are the temperature weighting functions for the surface and cold space, respectively. Conceptually, the weighting functions represent the absolute contribution of each level h to the observed brightness temperature.

It is often convenient to model the atmosphere as composed of a number of slabs. The vertical temperature within such a slab i is assumed to be determined by the temperature at some altitude h_i and a function such as a lapse rate. Under these assumptions, (4) assumes the form

$$T_B(\nu)=\sum_{i=1}^{N}T(h_i)W_i[\nu,R(\nu,T_{\text{surf}})]+T_{\text{surf}}W_{\text{surf}}[\nu,R(\nu,T_{\text{surf}})]+T_{\text{sky}}W_{\text{sky}}[\nu,R(\nu,T_{\text{surf}})], \quad (6)$$

where $W_i(\nu,R)$ is called the discrete weighting function for level i and is equal to

$$W_i(\nu,R(\nu,T_{\text{surf}}))=\int_{L_i}^{U_i}F_i[T(h),T(h_i)]\times W[h,\nu,R(\nu,T_{\text{surf}})]dh, \quad (7)$$

where L_i, U_i are the lower and upper boundaries of an atmospheric slab whose temperature structure is described by $T(h_i)$ and $F_i[T(h),T(h_i)]$ is the function relating $T(h)$ to $T(h_i)$ within slab i. By defining a vector $\mathbf{T}$ of temperatures that includes the $T(h_i)$, T_{surf} and T_{sky} and a similar vector $\mathbf{W}$ of discrete weighting functions, Eq. (6) may be expressed as the matrix equation

$$\mathbf{T}_B(\nu)=\mathbf{WT}. \quad (8)$$

The continuous weighting functions for the 1972 standard atmosphere at nadir and the extreme scan angle of the SCAMS instrument are shown in Fig. 1. Factors affecting the value of the weighting function include the absorption of the atmosphere at all levels and the reflectivity of the surface boundary. In the 50 GHz band used by the SCAMS instrument, the total absorption is dominated by oxygen, with minor contributions due to liquid water and water vapor. The discrete weighting functions for the SCAMS instrument computed for the 1965 supplemental atmospheres (Valley, 1965) using a 60°N winter atmosphere and the 15°N annual atmosphere are listed in Table 1. The difference in the weighting functions for these two atmospheres is a maximum of 10% over all channels and levels. This maximum difference occurs in the 1013–925 mb slab in the atmosphere for the lowest altitude SCAMS channel (52.85 GHz) and is due largely to the

difference between the water vapor concentrations at lower levels in these two model atmospheres. In higher altitude slabs or other channels, the variation is substantially less. Discrete weighting functions may thus be computed for a number of *a priori* climatologies with reasonable accuracy in all but perhaps the lowest levels of the atmosphere.

Of somewhat greater effect is the variation in the weighting functions with surface reflectivity. The difference between the weighting functions for land and ocean can be of the order of 30% for the lowest slabs for the 52.85 GHz oxygen channel of SCAMS. Higher altitudes and more opaque channels are again less affected. Fortunately, the form of the weighting function is linear with respect to surface emissivity. If the emissivity is known *a priori*, a simple interpolation between a surface emissivity of zero and a surface emissivity of one allows the weighting function to be obtained. Unfortunately, the reflectivity of the ocean surface is a function of its temperature. This causes the weighting functions, or Kalman-Bucy observation matrix, to be a function of one of the parameters to be estimated. This will be shown to require a Kalman-Bucy filter of extended form.

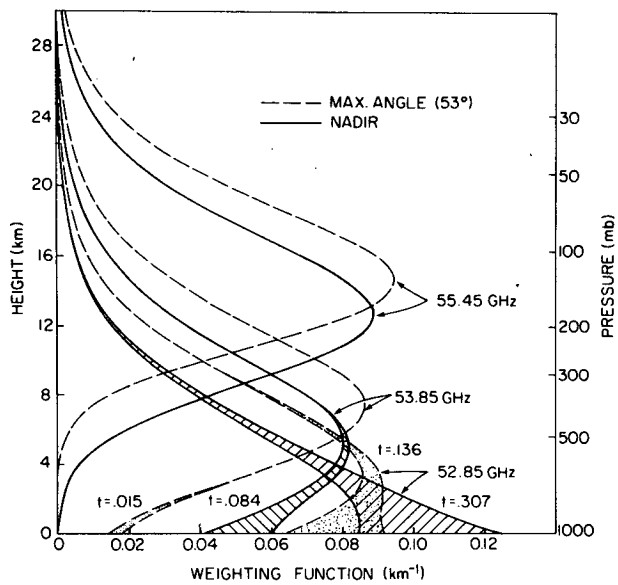

FIG. 1. SCAMS continuous weighting functions for the 1972 Standard Atmosphere at the extreme scan angle (53.5°, dashed line) and nadir (0°, solid line). The rightmost line at the surface for a given frequency/scan angle corresponds to the weighting function for a ocean surface (emissivity=0.45), the inner line corresponds to a land surface (emissivity=1). The value of t gives the total transmission of the atmosphere along the viewing angle.

3. Theory of the Kalman-Bucy filter

The theory of the discrete Kalman-Bucy filter has been widely discussed (Kalman, 1960; Leondes, 1970; Schweppe, 1973; Gelb, 1974). In order to provied a simple understanding of the operation of the filter and a definition of terms that are used later, this section is more heuristic and less mathematical than those sources. The notation that will be used is that of Gelb (1974). In this notation, quantities are often followed by a parenthesized minus or plus sign and are subscripted. The discrete time coordinate of the quantity is determined by the subscript. The parenthesized minus or plus signs refer to the values at time i before and after the processing of data received at time i. As is customary, the optimum estimate is denoted by a caret. Thus, the optimum estimate of A before the

TABLE 1. The discrete SCAMS weighting functions computed for a 60°N winter supplemental atmosphere and the difference between the weighting functions for the 60°N winter and 15°N annual supplemental atmospheres. The slab definition gives the quantities L_i and U_i used in (7).

	Channel 3 (52.85 GHz)		Channel 4 (53.85 GHz)		Channel 5 (55.45 GHz)		
Pressure (mb)	60°N Winter	Difference 60°N Winter 15°N Annual	60°N Winter	Difference 60°N Winter 15°N Annual	60°N Winter	Difference 60°N Winter 15°N Annual	Slab definition (mb)
Surface	0.285	0.032	0.078	0.010	0.000	0.000	Surface
1000	0.058	−0.006	0.030	−0.001	0.000	0.000	1013–925
850	0.135	0.011	0.076	−0.003	0.001	0.000	925–775
700	0.151	−0.011	0.139	−0.006	0.007	0.000	775–600
500	0.138	−0.004	0.173	−0.003	0.028	−0.001	600–450
400	0.086	−0.002	0.135	−0.004	0.058	−0.002	450–350
300	0.059	−0.001	0.106	−0.004	0.094	−0.002	350–275
250	0.035	0.001	0.069	−0.001	0.103	−0.001	275–225
200	0.030	0.000	0.065	0.000	0.145	−0.001	225–175
150	0.025	0.000	0.059	0.004	0.189	0.002	175–125
100	0.015	0.000	0.038	0.003	0.167	−0.003	125– 85
70	0.006	0.000	0.015	0.002	0.077	0.004	85– 60
50	0.006	0.000	0.014	0.001	0.080	0.002	60– 40
30	0.003	0.000	0.007	0.001	0.042	0.002	40– 20
10	0.001	0.000	0.002	0.000	0.013	0.001	20– 7.5

processing of data received at time i is $\hat{A}_i(-)$. The value of a parameter B after the processing of data received at time j is $B_j(+)$. It should be noted that although the coordinate of the data reception is referred to as "time," it is an arbitrary running coordinate. For remote profile sensing this coordinate is both spatial and temporal.

In order to develop the theory of the Kalman-Bucy filter, we will make the following assumptions: The process to be estimated is an n vector $\mathbf{X}_i$. This vector is assumed to have an expectation or mean conditioned on the time of the start of processing equal to $\hat{\mathbf{X}}_i(-)$. The error covariance of this conditional mean is assumed to be known and is an n by n matrix $\mathbf{P}_i(-)$. The observed process is represented by an m vector $\mathbf{Z}_i$ which is related to $\mathbf{X}_i$ by the linear relation

$$\mathbf{Z}_i=\mathbf{H}_i\mathbf{X}_i+\mathbf{N}_i, \tag{9}$$

where $\mathbf{H}_i$ is an m by n dimensional observation matrix and $\mathbf{N}_i$ is a zero mean white Gaussian process with covariance matrix $\mathbf{R}_i$.

Then, given that data has been observed at time 1, the optimum estimate of $\mathbf{X}_1$ using a simple Bayesian approach is

$$\hat{\mathbf{X}}_1(+)=\hat{\mathbf{X}}_1(-)+\mathbf{K}_1[\mathbf{Z}_1-\hat{\mathbf{Z}}_1(-)], \tag{10}$$

where

$$\hat{\mathbf{Z}}_1(-)=\mathbf{H}_1\hat{\mathbf{X}}_1(-), \tag{11}$$

$$\mathbf{K}_1=\mathbf{P}_1(-)\mathbf{H}_1^{\mathrm{T}}[\mathbf{H}_1\mathbf{P}_1(-)\mathbf{H}_1^{\mathrm{T}}+\mathbf{R}_1]^{-1}. \tag{12}$$

The *a posteriori* error covariance of the estimate will be given by

$$\mathbf{P}_1(+)=(\mathbf{I}-\mathbf{K}_1\mathbf{H}_1)\mathbf{P}_1(-), \tag{13}$$

where $\mathbf{I}$ is the n by n identity matrix. Being a Bayesian estimate, the estimate $\hat{\mathbf{X}}_1(+)$ will have the property that it is a conditional mean of $\mathbf{X}_1$, where the conditioning is now additionally on the fact that $\mathbf{Z}_1$ was observed.

The crucial point in the development of the filter now occurs if the process $\mathbf{X}_i$ is constrained to be a first-order Markovian process. In the discrete case at hand this implies that

$$\mathbf{X}_{i+1}=\mathbf{\Phi}_{i,i+1}\mathbf{X}_i+\mathbf{V}_i, \tag{14}$$

where $\mathbf{\Phi}_{i,i+1}$ is called the state transition matrix from time i to $i+1$ and represents the deterministic transition of $\mathbf{X}_i$, and $\mathbf{V}_i$ is a zero mean white Gaussian process, independent of $\mathbf{X}_i$, with covariance matrix $\mathbf{Q}_i$. It represents the truly random factors in the transition and is often called the plant noise. If a process is a first-order Markovian process, the conditional mean at time i may be propagated to time $i+1$ by

$$\hat{\mathbf{X}}_{i+1}(-)=\mathbf{\Phi}_{i,i+1}\hat{\mathbf{X}}_i(+) \tag{15}$$

and the error covariance of the mean by

$$\mathbf{P}_{i+1}(-)=\mathbf{\Phi}_{i,i+1}\mathbf{P}_i(+)\mathbf{\Phi}_{i,i+1}^{\mathrm{T}}+\mathbf{Q}_i. \tag{16}$$

These two equations then provide a means of obtaining the *a priori* conditional mean and its error covariance at time 2 from the *a posteriori* conditional mean (the estimate) and its error covariance at time 1. These quantities provide the necessary conditions to perform a Bayesian estimate at time 2. A recursive filter is thus obtained in which the estimate and its error covariance are fed forward and used in the next step.

It should be noted that nowhere in the development of the filter are any assumptions made concerning the stationarity of the processes. The matrices $\mathbf{Q}_i$, $\mathbf{H}_i$, $\mathbf{R}_i$ and $\mathbf{\Phi}_{i,i+1}$ may vary in either time or space and so nonstationary processes may be estimated using the Kalman-Bucy filter.

In a great many instances, the observed variables do not obey the linear relation (9). Rather, they obey some more general relation

$$\mathbf{Z}_i=h_i(\mathbf{X}_i)+\mathbf{N}_i. \tag{17}$$

If this is the case, some headway may be made by expanding $h_i(\mathbf{X}_i)$ around the *a priori* conditional mean at time i $[\hat{\mathbf{X}}_i(-)$ propagated by means of (15)] as

$$h_i(\mathbf{X}_i)=h_i[\hat{\mathbf{X}}_i(-)]+\mathbf{H}_i[\hat{\mathbf{X}}_i(-)][\mathbf{X}_i-\hat{\mathbf{X}}_i(-)]+\cdots, \tag{18}$$

where

$$\mathbf{H}_i[\mathbf{X}_i(-)]=\left.\frac{\partial h_i(\mathbf{X})}{\partial \mathbf{X}}\right|_{\mathbf{X}=\hat{\mathbf{X}}_i(-)}. \tag{19}$$

If higher order terms are neglected in this expansion, the method becomes one of linearizing about the expected operating point. If this approach is taken, Eqs. (10), (12) and (13) become, respectively,

$$\hat{\mathbf{X}}_i(+)=\hat{\mathbf{X}}_i(-)+\mathbf{K}_i\{\mathbf{Z}_i-h_i[\hat{\mathbf{X}}_i(-)]\}, \tag{20}$$

$$\mathbf{K}_i=\mathbf{P}_i(-)\mathbf{H}_i^{\mathrm{T}}[\hat{\mathbf{X}}_i(-)]\times\{\mathbf{H}_i[\hat{\mathbf{X}}_i(-)]\mathbf{P}_i(-)\mathbf{H}_i^{\mathrm{T}}[\hat{\mathbf{X}}_i(-)]+\mathbf{R}_i\}^{-1}, \tag{21}$$

$$\mathbf{P}_i(+)=\{\mathbf{I}-\mathbf{K}_i\mathbf{H}_i[\hat{\mathbf{X}}_i(-)]\}\mathbf{P}_i(-), \tag{22}$$

where $\hat{\mathbf{X}}_i(-)$ is again the estimate at time $i-1$ propagated forward to time i using (15).

In the context of passive remote temperature profile sensing, it is possible to associate a number of the matrices of the Kalman-Bucy filter with physical processes. The observation matrix $\mathbf{H}_i$ represents the discrete weighting function matrix of Section 2. In its more general form of (17), it represents the full equation of radiative transfer. $\mathbf{N}_i$ of course represents the instrumental noises. The state transition matrix $\mathbf{\Phi}_{i,i+1}$ represents the atmospheric dynamics while the plant noise $\mathbf{V}_i$ represents the uncertainties in the dynamics due to those factors which we are unable or unwilling to include. The virtue of the Kalman-Bucy filter is that it is able to utilize them in an optimum manner in a statistically rigorous setting.

4. Implementation

There are a large number of implementation considerations involved in the specification and design of a temperature-inverting Kalman-Bucy filter. Some are matters of pure choice, such as the causality of the filter, the number of scan angles to be inverted at once, etc. Some are matters of system identification and physical processes such as determining the state transition, plant noise and observation matrices. Others are matters of algorithm implementation so as to minimize adverse numerical effects. Finally, the problem of the possible lack of correspondence between models used in the filter and reality must be addressed.

The filter implemented was an extended filter capable of inverting up to five scan angles at once. This is accomplished by defining the vector $\mathbf{X}_i$ to be the temperatures at the 14 mandatory levels plus the surface at all the scan angles to be inverted. The brightness temperature of cold space was assumed to be constant and known *a priori*. The filter implemented was causal in the sense that it operated only on data in the "past" of the satellite path. Non-causal filters could have been implemented that use either a finite lag or the entire "future" history (see Gelb, 1974), but were not in the interests of simplicity. The SCAMS channels used in the inversion were chosen to be the three oxygen band channels. The use of the two lower frequency channels would have implied the additional requirement of inverting for liquid water and water vapor columns. This enhancement is being left to later filters.

The matter of system identification was attacked by using the National Meteorological Center K27 synoptic analysis grid and the various supplemental standard atmospheres. System identification is concerned with the identification of several matrices and the mean of the initial state at the start of processing. The matrices that are required to be determined are 1) $\mathbf{Q}_i$, the plant noise matrix; 2) $\mathbf{P}_i(-)$, the error covariance of the mean of the initial state; and 3) $\mathbf{\Phi}_{i,i+1}$, the state transition matrix.

The mean of the initial state was chosen to be specified by an interpolation in latitude on the standard supplemental atmospheres, which may be interpreted as climatological means. Given this specification of the mean of the initial state, its error covariance matrix $\mathbf{P}_i(-)$ was determined by comparison with actual prevailing conditions in January 1976 as reflected by the NMC K27 grid.

The specification of the state transition matrix and plant noise matrix are more difficult. To produce a statistical model to determine these quantities, it is necessary to obtain cross-covariances of temperatures at mandatory levels as a function of distance. While not unobtainable, this would have required an effort outoutside the scope of this project. This was likewise the case for a purely physical state transition matrix. The state transition matrix used was thus chosen to be a quasi-persistence transition. The prediction scheme at a single spot utilizes the level to be propagated and its adjacent levels. These adjacent levels are referenced to the level to be propagated through a climatological temperature lapse and a weighted average performed. The deviation of this average from climatology is then projected forward and the climatology reinserted. Likewise, the cross-scan components of the state transition matrix were chosen to perform a weighted average of the deviation from climatology at each level for adjacent spots. The weighting coefficients used in the filter were adjustable. In practice, it was found that the performance of the filter was relatively insensitive to their value.

Given the specification of the state transition matrix, it is possible to determine the plant noise matrix by a method similar to that used to determine $\mathbf{P}_i(-)$. A known state is projected forward using the state transition matrix and the error with respect to the known state at the "future" time is noted. The covariance of this error is the plant noise matrix. As a note, however, certain tests should be performed on this error to verify that it is indeed independent of $\mathbf{X}_i$.

The determination of the observation matrices was performed by computing the discrete weighting functions for the standard supplemental atmospheres for a number of altitudes and reflectivity cases. In the actual filter, the observation matrix was produced by an interpolation of these precomputed matrices. The value used for reflectivity over land was that inferred from the two SCAMS window channels. Over ocean, the value was determined using the predicted surface temperature (the propagated last estimate). This is necessary since the reflectivity of the ocean is a function of its temperature. This fact required that the filter be implemented as an extended filter with the determination of both $\mathbf{H}_i[\mathbf{X}_i(-)]$ and $h_i[\mathbf{X}_i(-)]$.

The numerical considerations of the algorithm are of vital importance in the implementation of the Kalman-Bucy filter. A simplistic implementation of the algorithm described in Section 3 will often diverge numerically. This is evidenced by the fact that the error covariance matrix $\mathbf{P}_i(+)$ ceases to be positive semi-definite, a requirement for any error covariance matrix. This has been often referred to as the divergence problem in Kalman filters (Fitzgerald, 1971; Gelb, 1974). One solution for this problem is to implement the algorithm in what is called the "square root algorithm" (Schmidt, 1970, Kaminski *et al.*, 1971). This form of the implementation is algorithmically equivalent to the formulation of Section 3 but provides equivalent additional precision in the computation of the Kalman gain $\mathbf{K}_i$ and the update of the error covariance matrices for measurement inclusion. Additionally, it guarantees that $\mathbf{P}_i(+)$ will be positive semi-definite at each step in the algorithm. It is again beyond the scope of this article to fully describe this formulation. The interested

TABLE 2. The mean error and rms error about the mean for the statistical D method and the single-spot Kalman inverter at three scan angles for the period 24–25 January 1976. These statistics are based on approximately 225 inversions at each scan angle.

	Extreme scan (Scan angle 0)				Mid-scan (Scan angle 3)				Nadir (Scan angle 6)			
	Statistical D		Kalman-Bucy		Statistical D		Kalman-Bucy		Statistical D		Kalman-Bucy	
Pressure (mb)	Mean error (K)	rms error (K)	Mean error (K)	rms error (K)	Mean error (K)	rms error (K)	Mean error (K)	rms error (K)	Mean error (K)	rms error (K)	Mean error (K)	rms error (K)
1000	8.2	11.6	2.2	7.1	5.5	8.3	1.3	6.2	5.7	8.1	1.7	5.4
850	2.0	4.6	0.7	3.0	2.3	3.5	1.6	3.5	2.3	3.9	2.2	3.3
700	1.1	3.0	0.5	1.2	1.5	2.6	1.4	2.0	1.6	2.3	1.9	2.0
500	− 0.7	2.8	−0.2	1.7	− 0.7	2.7	0.0	1.8	− 0.5	2.6	0.1	1.7
400	− 1.2	3.0	0.9	1.7	− 1.6	3.3	0.5	2.7	− 1.3	3.3	0.5	2.5
300	− 1.7	3.5	1.0	2.3	− 3.3	4.0	−0.1	3.3	− 2.8	4.0	−0.4	3.2
250	− 1.9	3.9	−0.4	3.3	− 4.3	4.6	−1.6	4.0	− 4.1	4.6	−2.0	3.9
200	0.9	2.8	−1.7	2.8	− 1.0	3.5	−2.6	3.0	− 1.3	3.0	−2.9	2.8
150	3.1	1.9	−1.6	1.8	2.8	2.3	−1.5	1.6	2.5	2.3	−1.4	1.5
100	5.6	3.3	2.0	1.5	6.4	3.8	2.9	3.0	5.9	3.7	3.2	2.9
70	2.1	3.2	0.3	2.3	2.8	3.6	1.3	3.6	2.6	4.1	1.5	3.5
50	1.8	3.3	0.8	2.0	2.1	4.0	2.0	3.7	2.1	4.5	1.8	3.8
30	− 1.2	4.6	−0.3	3.2	− 1.5	4.8	0.3	4.6	− 1.5	5.2	0.1	4.3
10	−10.1	6.6	−5.3	6.3	−11.5	5.8	−4.5	7.3	−12.3	5.9	−5.4	7.8

reader is referred to the previously mentioned references for an excellent review.

The final consideration in the implementation of the algorithm is the presence of modeling errors in its construction. This is especially important in the case of the discrete weighting functions. The weighting functions are determined numerically using certain assumptions on the absorption models, vertical temperature structure, etc. Since the update of the predicted profiles is driven from the difference between the actual observation and the predicted observation, it is important that the expectation of the difference between the actual brightness temperatures and the brightness temperatures using the actual profile in conjunction with the discrete weighting functions be zero. To remove any bias in this area an empirical correction was included in the filter. This correction was constructed using several days of NMC synoptic analysis matched with SCAMS observations.

5. Results

The implemented Kalman-Bucy filter was exercised on two periods of SCAMS data that could be matched with the NMC K27 grid (24–25 January 1976 and 3–6 February 1976). A summary of the mean error and the rms error about the mean of the retrievals for sur-

TABLE 3. As in Table 2 except for 3–6 February 1976. These statistics are based on approximately 650 inversions at each scan angle.

	Extreme scan (Scan angle 0)				Mid-scan (Scan angle 3)				Nadir (Scan angle 6)			
	Statistical D		Kalman-Bucy		Statistical D		Kalman-Bucy		Statistical D		Kalman-Bucy	
Pressure (mb)	Mean error (K)	rms error (K)	Mean error (K)	rms error (K)	Mean error (K)	rms error (K)	Mean error (K)	rms error (K)	Mean error (K)	rms error (K)	Mean error (K)	rms error (K)
1000	6.7	9.4	0.0	3.8	4.8	7.7	0.0	3.9	4.6	7.5	−0.6	4.4
850	1.0	3.7	0.3	2.4	1.5	3.1	0.8	2.4	1.5	2.9	0.3	2.6
700	0.5	2.4	1.0	1.7	1.1	2.1	1.2	1.8	1.2	2.2	1.0	1.9
500	−0.8	2.0	0.3	1.5	−0.4	2.3	0.2	1.8	−0.4	2.4	−0.1	1.8
400	−1.0	2.2	1.3	2.0	−1.0	2.7	0.8	2.2	−1.1	2.7	0.7	2.4
300	−1.4	3.4	1.2	3.4	−2.1	3.9	0.5	3.6	−2.5	4.0	0.1	3.8
250	−1.5	3.9	0.0	3.6	−2.6	4.2	−0.1	4.0	−3.0	4.1	−0.5	4.1
200	0.6	3.3	−1.6	2.7	−0.7	3.2	−1.6	2.9	−0.9	3.0	−1.5	2.9
150	1.9	2.4	−1.3	1.6	1.2	2.3	−1.1	1.4	1.4	2.6	−1.1	1.4
100	4.6	2.7	2.3	2.0	4.4	3.3	2.6	2.4	4.8	3.6	2.9	2.7
70	1.9	2.7	0.2	2.0	2.1	3.5	0.3	3.1	2.3	3.6	0.5	3.7
50	1.5	3.0	0.2	3.0	1.8	3.0	0.7	4.4	1.9	3.4	1.0	5.2
30	0.3	4.6	−0.1	4.8	0.6	4.1	0.6	6.1	0.7	4.9	1.1	6.8
10	−6.8	9.1	−1.9	10.4	−6.0	8.6	−0.4	11.5	−5.7	8.4	0.1	12.2

TABLE 4. The mean error and rms error about the mean for a two-spot Kalman inverter operating at extreme scan (scan angles 0 and 1) and at close scan (scan angles 5 and 6) for the period 24–25 January. These statistics are based on approximately 225 inversions at each scan angle.

	Extreme scan				Close scan			
	Scan angle 0		Scan angle 1		Scan angle 5		Scan angle 6	
Pressure (mb)	Mean error (K)	rms error (K)	Mean error (K)	rms error (K)	Mean error (K)	rms error (K)	Mean error (K)	rms error (K)
1000	4.0	6.7	3.8	7.1	1.4	5.1	1.9	5.2
850	1.3	2.4	1.7	3.1	2.0	3.2	2.3	3.1
700	0.8	0.8	1.3	1.5	1.7	2.1	1.9	1.9
500	−0.1	1.9	0.2	1.7	0.1	1.6	0.0	1.5
400	0.8	1.8	0.9	1.8	0.6	2.3	0.4	2.2
300	0.4	2.5	0.2	2.6	−0.1	3.1	−0.5	3.1
250	−1.5	3.3	−1.6	3.3	−1.7	4.0	−2.0	4.0
200	−2.9	2.6	−2.8	2.4	−2.6	2.9	−2.9	2.9
150	−2.4	2.0	−2.1	1.7	−1.4	1.4	−1.3	1.4
100	1.9	1.8	2.4	1.8	3.2	3.0	3.5	2.9
70	1.0	2.0	1.3	2.2	1.4	3.7	1.8	3.5
50	1.6	2.4	1.7	2.6	1.8	3.9	2.2	3.6
30	0.8	3.8	0.5	4.2	0.0	4.6	0.4	4.1
10	−5.0	7.6	−5.1	8.1	−5.4	7.6	−5.1	7.7

face elevations of less than 1 km are summarized in Tables 2–7. The ground truth used to determine these errors was the NMC K27 grid in data-rich regions. These data-rich areas are essentially those of Waters (1975) and are shown in Fig. 2. Geographically, they are Japan, the United States, Canada and Europe. The entries in Tables 2–7 are for several configurations of the Kalman filter and for the present statistical D method of inversion. The configurations tested were the single spot inverter and bulk inverters in which two and three scan angles were inverted simultaneously. Figs. 3–6 summarize the rms performance about the mean of the single spot inverter, the bulk two-spot inverter and the statistical D matrix method of inversion for the periods investigated.

The results indicate that the Kalman-Bucy filter outperforms the statistical D at all lower levels in the atmosphere below 70 mb. This is true both with regard to the mean error and rms error about the mean. The Kalman filter shows a substantial elimination of the mean error at all levels except those around tropopause. The occurrence of mean errors at these levels is not well understood at present. The inferior performance of the Kalman-Bucy filter above 70 mb is due to the lack of SCAMS weighting functions above this altitude. Under these conditions, the statistical D matrix retrievals are dominated by the *a priori* mean. The Kalman filter, however, runs in an open loop mode with little correction due to observed data. The effect of imperfect state identification is magnified under these conditions.

TABLE 5. As in Table 4 except for the period 3–6 February 1976. These statistics are based on approximately 650 inversions at each scan angle.

	Extreme scan				Close scan			
	Scan angle 0		Scan angle 1		Scan angle 5		Scan angle 6	
Pressure (mb)	Mean error (K)	rms error (K)	Mean error (K)	rms error (K)	Mean error (K)	rms error (K)	Mean error (K)	rms error (K)
1000	0.0	4.0	0.2	4.1	−0.2	4.3	−0.4	4.5
850	0.3	2.3	0.4	2.2	0.6	2.6	0.5	2.7
700	0.9	1.6	1.0	1.5	1.1	1.8	1.0	1.8
500	0.3	1.5	0.2	1.5	−0.1	1.6	−0.2	1.6
400	1.3	1.8	1.1	1.9	0.5	2.2	0.5	2.2
300	1.2	3.0	0.8	3.0	0.0	3.6	0.1	3.7
250	0.0	3.2	0.0	3.3	−0.6	4.0	−0.6	4.1
200	−1.6	2.5	−1.6	2.4	−1.8	2.9	−1.7	3.1
150	−1.3	1.7	−1.2	1.5	−1.1	1.5	−1.0	1.6
100	2.3	2.2	2.5	2.1	2.9	2.7	3.0	2.7
70	0.1	1.8	0.3	2.0	0.7	3.6	0.6	3.8
50	0.0	2.8	0.4	2.8	1.3	5.1	1.1	5.4
30	−0.3	4.7	0.0	4.6	1.4	6.8	1.2	7.2
10	−2.2	10.0	−1.6	9.8	0.7	11.9	0.2	12.4

TABLE 6. The mean error and rms error about the mean for a three-spot Kalman inverter operating at extreme scan (scan angles 0, 1, 2) and at close scan (scan angles 5, 6, 7) for the period 24–25 January, 1976. These statistics are based on approximately 225 inversions at each scan angle.

	Extreme scan						Close scan					
	Scan angle 0		Scan angle 1		Scan angle 2		Scan angle 5		Scan angle 6		Scan angle 7	
Pressure (mb)	Mean error (K)	rms error (K)	Mean error (K)	rms crror (K)	Mean error (K)	rms error (K)	Mean error (K)	rms error (K)	Mean error (K)	rms error (K)	Mean error (K)	rms error (K)
1000	2.3	6.8	2.5	6.7	2.3	6.1	1.4	5.0	1.9	5.0	2.4	5.5
850	0.9	2.6	1.8	2.9	2.0	2.9	1.9	3.2	2.4	3.1	2.7	3.3
700	0.6	1.0	1.4	1.5	1.6	1.8	1.6	2.0	1.9	1.9	2.0	1.9
500	−0.3	1.7	−0.1	1.7	0.0	1.8	0.1	1.5	0.0	1.3	−0.1	1.4
400	0.7	1.6	0.6	1.8	0.6	2.0	0.6	2.1	0.4	2.0	0.1	2.1
300	0.8	2.6	0.3	2.6	−0.1	2.6	−0.2	3.1	−0.5	3.1	−0.8	3.2
250	−0.6	3.8	−1.0	3.8	−1.4	3.7	−1.7	4.1	−2.0	4.1	−2.3	4.1
200	−1.9	3.3	−2.2	3.3	−2.4	3.2	−2.6	3.0	−2.0	2.9	−3.1	3.0
150	−1.7	2.3	−1.5	2.0	−1.6	2.0	−1.4	1.5	−1.3	1.4	−1.1	1.6
100	2.0	1.9	2.4	2.2	2.6	2.5	3.2	3.0	3.5	2.9	3.0	2.8
70	0.7	2.5	0.9	2.6	1.0	2.7	1.4	3.7	1.8	3.5	2.2	3.4
50	1.5	2.7	1.6	2.7	1.7	2.9	1.9	4.0	2.2	3.6	2.6	3.4
30	0.8	3.9	0.3	4.0	0.1	4.2	0.1	4.7	0.4	4.2	0.8	3.9
10	−4.1	7.0	−4.5	7.5	−4.8	8.0	−5.3	7.5	−5.0	7.6	−4.6	7.6

A comparison of the various Kalman-Bucy filters as a function of scan angle shows that, for SCAMS data, the performance increases with increasing scan angle. The inversions at the extreme scan angle (those including scan angle 0, at 53.5°) outperform those at mid-scan (scan angle 3, at 25.6°) and nadir (angle 6, at 0°). The cause of this effect is the increase in altitude of the peak of the weighting functions with increasing scan angle. As the weighting functions lift, a combined effect occurs. Because the instrument "sees" more of the atmosphere, the observed brightness temperatures are thus more directly produced by the variables whose values are desired in the ultimate inversion. As the instrument "sees" less of the surface, uncertainties in both the surface elevation and emissivity have a smaller effect.

A comparison of the various configurations (one-, two- and three-spot inverters) show that the multi-spot bulk inverters have improved accuracies when compared with the single-spot inverter. This improvement comes from several sources. First, since the weighting functions differ with scan angle, the use of several scan angles increases the number of weighting functions available to the inversion from a fixed number of observation frequencies. Second, instrumentation noise is essentially averaged over the scan angles, thus reducing it. Finally, surface uncertainties are reduced by a similar averaging process. The occasional occurrence

TABLE 7. As in Table 6 except for the period 3–6 February 1976. These statistics are based on approximately 650 inversions at each scan angle.

	Extreme scan						Close scan					
	Scan angle 0		Scan angle 1		Scan angle 2		Scan angle 5		Scan angle 6		Scan angle 7	
Pressure (mb)	Mean error (K)	rms error (K)	Mean error (K)	rms error (K)	Mean error (K)	rms error (K)	Mean error (K)	rms error (K)	Mean error (K)	rms error (K)	Mean error (K)	rms error (K)
1000	0.1	4.1	−0.2	3.8	−0.1	3.9	−0.6	4.7	−1.0	4.7	−1.1	4.4
850	0.5	2.3	0.5	2.1	0.5	2.4	0.0	3.0	−0.3	2.9	−0.3	2.7
700	1.0	1.5	0.9	1.3	0.9	1.6	0.5	2.2	0.4	2.0	0.3	2.0
500	0.3	1.5	0.1	1.2	0.0	1.2	−0.3	1.7	−0.4	1.7	−0.5	1.8
400	1.3	1.6	1.0	1.5	1.0	1.5	0.6	2.3	0.5	2.3	0.4	2.3
300	1.3	2.6	1.1	2.9	0.9	3.1	0.6	3.9	0.5	3.8	−0.6	3.9
250	0.0	3.2	0.1	3.4	−0.1	3.5	−0.4	3.8	−0.5	3.8	−0.6	3.9
200	−1.5	2.4	−1.5	2.2	−1.8	2.0	−1.8	2.4	−1.8	2.5	−1.9	2.6
150	−1.2	2.0	−1.1	1.7	−1.1	1.5	−1.1	1.5	−1.1	1.4	−1.1	1.5
100	2.3	2.3	2.5	2.2	2.7	2.2	2.9	2.6	3.0	2.7	3.0	2.7
70	−0.1	1.9	0.3	1.9	0.4	2.2	0.9	3.0	0.9	3.1	0.9	3.2
50	−0.1	2.9	0.5	2.9	0.9	3.1	1.8	4.2	1.8	4.4	1.7	4.6
30	0.6	4.6	0.9	4.6	1.4	4.6	2.7	5.1	2.7	5.1	2.6	5.3
10	1.7	6.5	2.2	6.9	2.3	7.2	2.5	9.1	2.3	9.2	2.2	9.9

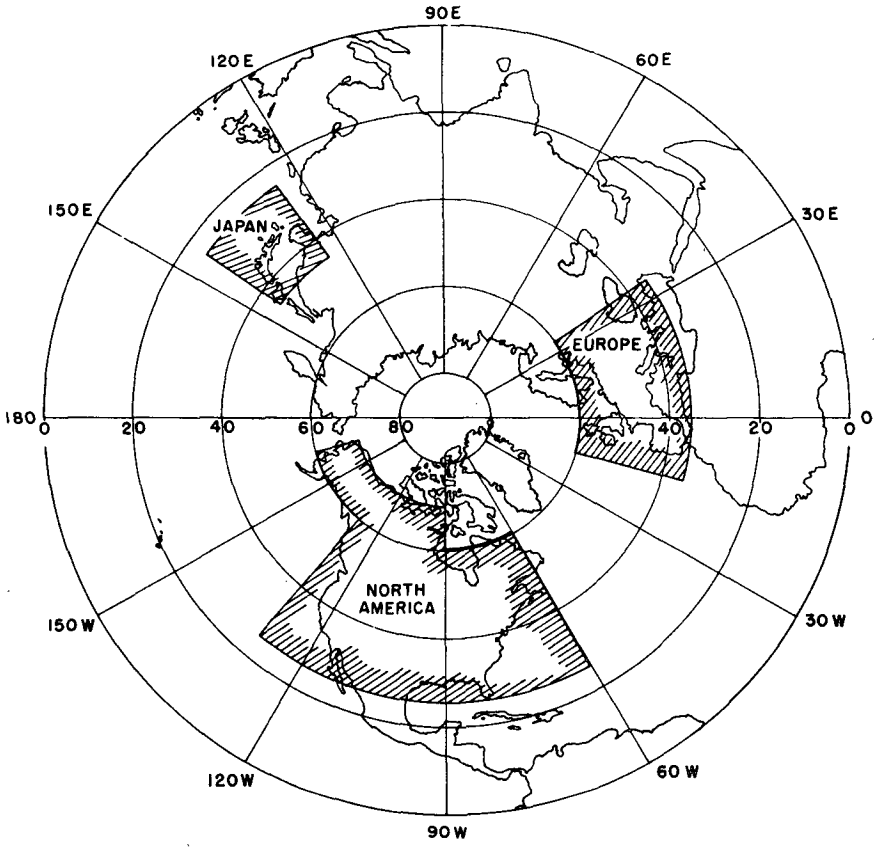

FIG. 2. Regions of the National Meteorological Center K27 analysis grid used for verification (hatched areas) in this paper.

of degraded performance in the multi-spot retrieval is thought to be caused by artifacts in the data.

The period chosen here for testing should be regarded as a worst case for both Kalman-Bucy filter and statistical D method performance. Waters (1975) has shown that the performance of the statistical D method improves during other seasons. During midwinter, the existence of severe storm patterns lowers the spatial coherency of the atmosphere. As it is this coherency that allows the Kalman-Bucy filter to outperform the statistical D method, a more marked improvement should be observed in other seasons.

During testing, the filter remained stable for the duration of all data processed. Occasionally, a very short period of poor performance was noted at the start of data processing. An instance of such a transient behavior is shown in Fig. 7. In the typical cases shown, the filter has achieved acceptable performance within three inversions.

6. Complexity considerations

For routine usage in an operational setting, the Kalman-Bucy filter described must be modified. The algorithm requires order of n^3 plus order of n^2r multiplications (Kaminski *et al.*, 1971), where n is the number of parameters to be estimated and r the number of input observations. For $n>r$, this complexity is dominated by the order of n^3 term. Since the number of parameters in a multi-spot retrieval is proportional to the number of scan angles processed, higher order inverters become impractical after some point.

Two alternatives exist for reducing the computational burden. The first is a reduction in the number of variables to be estimated by a process such as a truncated Karhunen-Loève expansion. Due to the fact that the processes are assumed to be nonstationary, this state reduction will generally be of a more complex form than the usual rotation using the eigenvectors of a single a priori covariance matrix.

A second alternative that allows a reduction in complexity is a suboptimal filter design in which certain matrices are precomputed. The order of n^3 term in the complexity of the filter is produced by the propagation and update of the error covariance. A precomputation of the error covariance along a nominal satellite track may be made if the expected variation of the value of the observation matrix along the track is small. This elimination of the on-line propagation and update of the error covariance matrix would result in a savings of over 50% in the filter implemented. In a similar

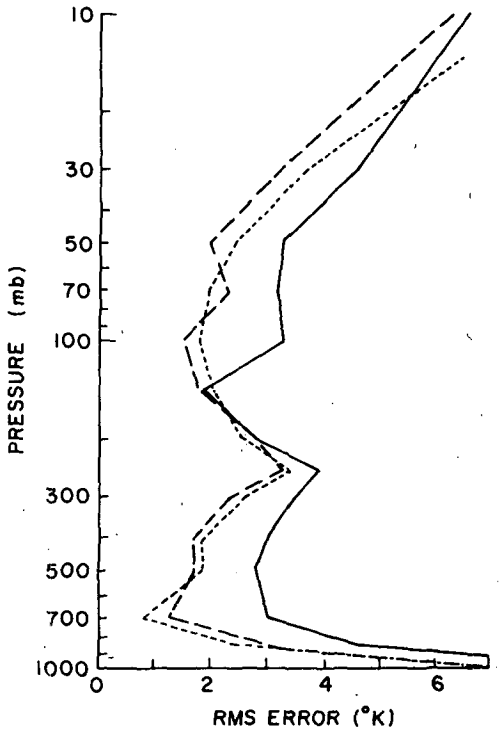

FIG. 3. Plots of the rms error about the mean at scan angle 0 (53.5°) for the statistical D inversions (solid line), one-spot Kalman inverter (long-dashed line), and two-spot Kalman inverter (short-dashed line) for the period 25–26 January 1976.

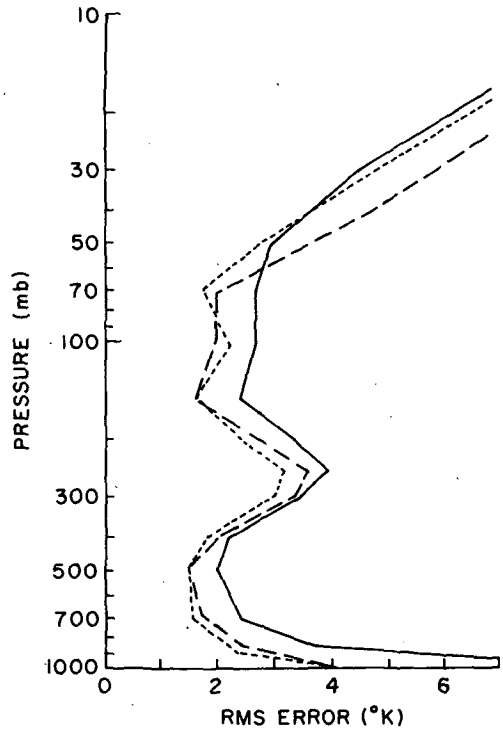

FIG. 5. Plots of the rms error about the mean at scan angle 0 (53.5°) for the statistical D inversions (solid line), one-spot Kalman inverter (long-dashed line), and two-spot Kalman inverter (short-dashed line) for the period 3–6 February 1976.

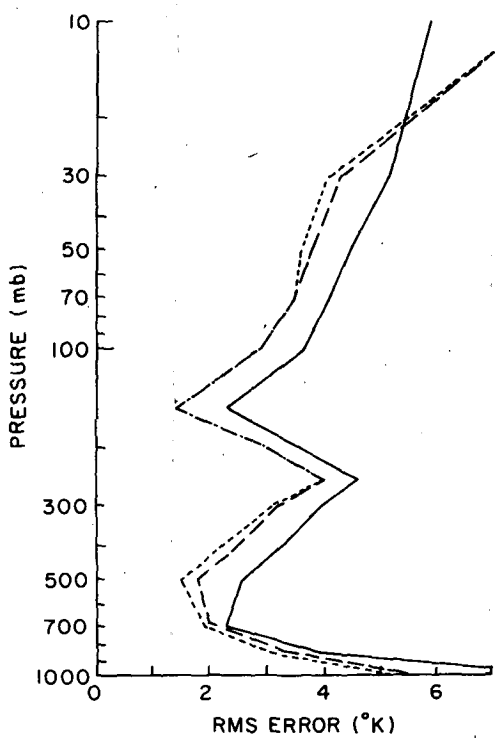

FIG. 4. Plots of the rms error about the mean at scan angle 6 (0°) for the statistical D inversions (solid-line), one-spot Kalman inverter (long-dashed line), and two-spot Kalman inverter (short dashed line) for the period 25–26 January 1976.

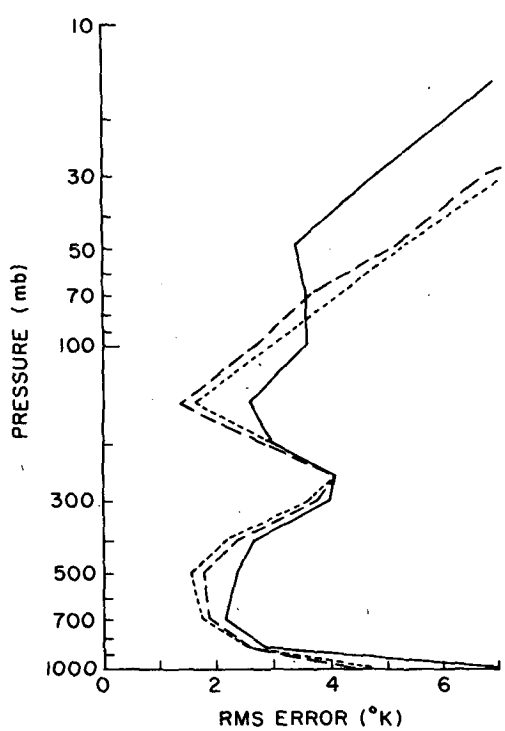

FIG. 6. Plots of the rms error about the mean at scan angle 6 (0°) for the statistical D inversions (solid line), one-spot Kalman inverter (long-dashed line), and two-spot Kalman inverter (short-dashed line) for the period 3–6 February 1976.

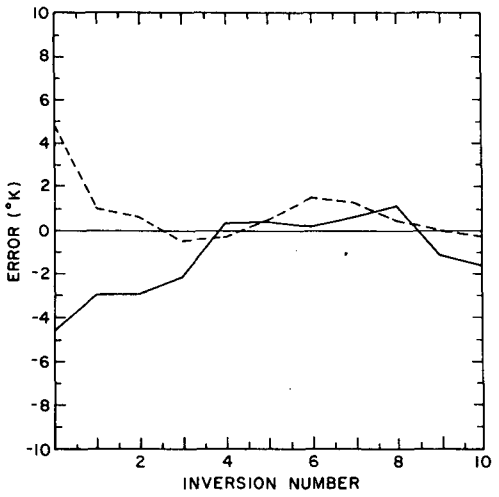

FIG. 7. Two transient responses of the one-spot Kalman filter at 700 mb showing initial poor performance.

manner, a suboptimal filter in which the Kalman gain is also precomputed may be designed. If precomputed Kalman gains are used, the speed of the Kalman-Bucy filter approximates that of the statistical D method. A full discussion of the mathematical implications of such a matrix precomputation is given in Gelb (1974).

7. Summary and conclusions

The extended Kalman-Bucy filter has been shown to be a valuable technique in the context of temperature profile inversion using the SCAMS instrument. Substantial improvement has been demonstrated over a previously used inversion method.

Conceptually, the filter has many advantages such as modularity and the ready identification of the roles of atmospheric dynamics, radiative transfer and statistical theory in the overall inversion process. This modularity also has practical aspects. To define a new Kalman-Bucy filter for an instrument with the same scan geometry but a different set of channel frequencies, one need only generate a new set of discrete weighting functions.

The Kalman filter should provide a valuable new tool in the area of remote atmospheric parameter retrieval.

Acknowledgments. The authors wish to thank Dr. P. W. Rosenkranz for the SCAMS brightness temperature and statistical D inversion data. The observation matrices were computed using a number of his routines. Special thanks is extended to Dr. D. Gustafson of Scientific Systems Inc., Cambridge, MA for many conversations on Kalman-Bucy filtering and its square root implementation. This work was supported under NASA Contract NAS5-21980.

REFERENCES

Fitzgerald, R. J., 1971: Divergence of the Kalman filter. *IEEE Trans. Auto. Control*, **AC-16**, 736–747.

Fleming, H. E., and W. L. Smith, 1972: Inversion techniques for remote sensing of atmospheric temperature profiles. *Proc. Fifth Symp. Temperature*, Pittsburgh, Instrum. Soc. Amer., 2239–2250.

Gelb, A., Ed., 1974: *Applied Optimal Estimation*. The MIT Press, 347 pp.

Grody, N. C., and P. P. Pellegrino, 1977: Synoptic scale studies using the Nimbus 6 scanning microwave radiometer. *J. Appl. Meteor.*, **16**, 816–826.

Kalman, R. E., 1960: A new approach to linear filtering and prediction problems. *Trans. ASME*, **88D**, 35–70.

Kaminski, P. G., A. E. Bryson and S. F. Schmidt, 1971: Discrete square root filtering: A survey of current techniques. *IEEE Trans. Auto. Control*, **AC-16**, 727–736.

Leondes, C. F., Ed., 1970: Theory and applications of Kalman filtering. NATO Advisory Group for Aerospace Research and Development [NTIS No. AD-704306].

Schmidt, S. F., 1970: Computational techniques in Kalman filtering. NATO Advisory Group for Aerospace Research and Development, pp. 67–86 [NTIS No. AD-704306].

Rosenkranz, P. W., F. T. Barath, J. C. Blinn, E. J. Johnston, W. B. Lenoir, D. H. Staelin and J. W. Waters, 1972: Microwave radiometer measurements of atmospheric temperature and water from an aircraft. *J. Geophys. Res.*, **77**, 5833–5844.

Schweppe, F. C., 1973: *Uncertain Dynamic Systems*. Prentice Hall, 563 pp.

Staelin, D. H., 1969: Passive remote sensing at microwave wavelengths. *Proc. IEEE*, **57**, 427–439.

——, A. H. Barrett, P. W. Rosenkranz, F. T. Barath, E. J. Johnston, J. W. Waters, A. Wouters and W. B. Lenoir, 1975: The scanning microwave spectrometer (SCAMS) experiment. *The Nimbus 6 Users Guide*, Goddard Space Flight Center, Greenbelt, Md., 59–86.

——, P. W. Rosenkranz, F. T. Barath, E. J. Johnston and J. W. Waters, 1977: Microwave spectroscopic imagery of the Earth. *Science*, **197**, 991–993.

Valley, S. L., Ed., 1965: *Handbook of Geophysics and Space Environments*. Air Force Cambridge Research Laboratories, 637 pp.

Waters, J. W., K. F. Kunzi, R. L. Pettyjohn, R. K. L. Poon and D. H. Staelin, 1975: Remote sensing of atmospheric temperature profiles with the Nimbus 5 microwave radiometer. *J. Atmos. Sci.*, **32**, 1953–1969.